

Iridium-Based Ultramicroelectrode Array Fabricated by Microlithography

Samuel P. Kounaves,¹ Wen Deng, and Pamela R. Hallock

Department of Chemistry, Tufts University, Medford, Massachusetts 02155

Gregory T. A. Kovacs and Christopher W. Storment

Center For Integrated Systems, Stanford University, Room CIS 130, M/C 4070, Stanford, California 94305

A microlithographically fabricated iridium ultramicroelectrode array is used to provide a disk array for formation of mercury microhemispheres. The mercury ultramicroelectrode array (Hg UMEA) shows a response with chronoamperometry and square wave anodic stripping voltammetry equivalent to that expected for a single Hg UME. The array, made up of 19 interconnected 10- μm -diameter UMEs, provides a multiplication of the signal current proportional to the number of UMEs in the array, without any indications of overlap of the diffusion fields. Deposited mercury on the iridium disks is physically and chemically stable with no indication of degradation or dissolution of the iridium pads even after several days of use. This microlithographically fabricated device provides a stable, well-defined, and reproducible array of mercury ultramicroelectrodes. The analytical utility and performance of the Hg UMEA is demonstrated by the analysis of Cd(II), Pb(II), and Cu(II) in neat spring water samples.

The highly advantageous properties of ultramicroelectrodes (UMEs) in general^{1–3} and of mercury UMEs in particular^{4–8} have been well documented. However, the major drawbacks for their practical use in laboratory and environmental field analyses are the subnanoampere currents which comprise the faradaic electroanalytical signal and, for mercury UMEs, the apparent inability to obtain a rugged and stable configuration of mercury on an inert substrate and the solubility of metal substrates such as platinum and gold in mercury.^{5,9}

To overcome the low-current problem, a variety of UME arrays have been fabricated and characterized over the past

decade.^{10–24} They have been produced by such techniques as photolithography, electrodeposition, and mechanical assembly. They have been made from metals such as Pt, Au, and Cr, various forms of carbon, semiconductor materials, and oxides.

One of the first to report fabrication and “electroanalytically based” experimental work using the microelectrode array concept was that of Matsuda and his group to confirm the theory for chronopotentiometry and chronoamperometry at partially covered electrodes (i.e., in effect, an array of microelectrodes).¹⁰ Using a photolithographic process and mask for the array pattern, they fabricated hexagonal array of exposed “gold microelectrodes” on the electrode surface. Later, Aoki and Osteryoung¹¹ used a similar technique to produce, on a large glassy carbon substrate, arrays of circular microelectrodes with radii of 20, 40, 100, and 200 μm , respectively. Wightman¹² and his group constructed an electrode array using five rows of 20 carbon fibers sandwiched between glass slides, resulting in 10- μm -diameter disks. The electrode was used as a channel-type amperometric flow cell detector. Sleszynski and Osteryoung¹³ used epoxy-filled reticulated vitreous carbon (RVC) to construct a two-dimensional random-order microelectrode array that yielded nearly steady-state currents. Hepel and Osteryoung¹⁴ made Cr and Au microelectrode arrays with over one million active electrodes on a 1- cm^2 area, each of 0.75- μm diameter, using

- (1) Wightman, R. M.; Wipf, D. O. In *Electroanalytical Chemistry*; Bard, A. J., Ed.; Marcel Dekker: New York, 1989; Vol. 15, pp 267–353.
(2) Fleischmann, S.; Pons, S.; Rolison, D. R.; Schmidt, P. P. Ultramicroelectrodes; DataTech Systems: Morganton, NC, 1987.
(3) Andrieux, C. P.; Hapiot, P.; Savéant, J.-M. *Electroanalysis* 1990, 2, 183–193.
(4) Wehmeyer, K. R.; Wightman, R. M. *Anal. Chem.* 1985, 57, 1989–1993.
(5) Baranski, A. S. *Anal. Chem.* 1987, 59, 661–666.
(6) Daniele, S.; Baldo, M. A.; Ugo, P.; Mazzocchini, A. *Anal. Chem. Acta* 1989, 219, 9–18.
(7) Kounaves, S. P. *Anal. Chem.* 1992, 64, 2998–3003.
(8) Kounaves, S. P.; Deng, W. *Anal. Chem.* 1993, 65, 375–379.
(9) Pons, J.; Daschbach, J.; Pons, S.; Fleischmann, M. *J. Electroanal. Chem.* 1988, 239, 427–431.
(10) Gueshi, T.; Tokuda, K.; Matsuda, H. *J. Electroanal. Chem.* 1978, 89, 247–260.
(11) Aoki, K.; Osteryoung, J. J. *Electroanal. Chem.* 1981, 126, 315–320.
(12) Caudill, W. L.; Howell, J. O.; Wightman, R. M. *Anal. Chem.* 1982, 54, 2532–2535.
(13) Sleszynski, N.; Osteryoung, J.; Carter, M. *Anal. Chem.* 1984, 56, 130–135.
(14) Hepel, T.; Osteryoung, J. J. *Electrochem. Soc.* 1986, 133, 752–757.
(15) Uosaki, K.; Okazaki, K.; Kita, H.; Takahashi, H. *Anal. Chem.* 1990, 62, 652–656.
(16) Miller, C. J.; Majda, M. *J. Electroanal. Chem.* 1986, 207, 49–72.
(17) Morita, K.; Shimizu, Y. *Anal. Chem.* 1989, 61, 159–162.
(18) Penner, R. M.; Martin, C. R. *Anal. Chem.* 1987, 59, 2625–2630.
(19) Thormann, V.; van den Bosch, P.; Bond, A. M. *Anal. Chem.* 1985, 57, 2764–2770.
(20) Bond, A. M.; Henderson, T. L. E.; Thormann, W. *J. Phys. Chem.* 1986, 90, 2911–2917.
(21) Fosdick, L. E.; Anderson, J. L.; Baginski, T.; Jaeger, R. C. *Anal. Chem.* 1986, 58, 2750–2756.
(22) Matsue, T.; Aoki, A.; Ando, E.; Uchida, I. *Anal. Chem.* 1990, 62, 409–411.
(23) Glass, R. S.; Perone, S. P.; Ciarlo, D. R. *Anal. Chem.* 1990, 62, 1914–1918.
(24) Samuelsson, M.; Armgarth, M.; Nylander, C. *Anal. Chem.* 1991, 63, 931–936.

electron beam lithography and poly(methyl methacrylate) resist. Several groups have used porous materials such as polycarbonate membrane or aluminum oxide films either to fabricate recessed random "microhole" arrays¹⁵⁻¹⁷ or, in one case, to electrodeposit platinum into the pores resulting in random-ordered 0.1-μm disk microelectrodes.¹⁸ A substantial amount of work has also been done with so-called band arrays or linear microelectrode arrays. These band array electrodes have one of their dimensions in the microsized domain, while the other dimension may be several orders of magnitude larger. They have usually been fabricated either by sandwiching a thin metal layer between glass layers and then polishing one end^{19,20} or by photolithography.²¹⁻²⁴ In spite of the variety and numbers of UME arrays investigated, nothing appears in the literature in reference to fabrication or studies involving a mercury UME array even though the mercury electrode has been, and continues to be, the overwhelming substrate of choice since the introduction of polarography.

To best reproduce the behavior of a *single* microelectrode, the *array* of microelectrodes must consist of *well-separated, ordered, disk* elements. The only fabrication technique which offers the required resolution and control to produce such UME arrays is the photolithographic technology used for integrated circuit (IC) manufacture. Using such technology it would be easy to produce an array of micrometer-sized disks (pads) of platinum and gold. However, the formation of mercury hemisphere UMEs on these two commonly used metals would result in the amalgamation and rapid delamination of the pad from the silicon substrate. Thus, even though Pt and Au IC-based arrays have been made, they are not suitable for the formation of stable mercury UMEs. Band UMEs made of these metals are not amenable to use as substrates for mercury film formation, since coverage of such a long line would require amalgamation (which of course is undesirable) and mercury deposition on inert substrates would result in a long column of easily detachable mercury spheres. In addition, band UMEs do not attain a truly time-invariant steady-state current regimes as do inlaid disk UMEs.²⁵

It has been shown that iridium is an excellent substrate on which to form a mercury film or semisphere. Unlike platinum, gold, or silver, the solubility of iridium in mercury is well below 10⁻⁶ wt %,^{26,27} and thus neither iridium dissolution nor intermetallic compound formation between the iridium and mercury occurs. In addition, it has been shown that the properties of the mercury vis-à-vis the iridium surface (i.e., Hg-solution surface tension in relation to the Hg-Ir surface energy) inherently favor the formation of a stable well-adhering mercury semisphere on micrometer-sized iridium disks. Several papers have been published describing the fabrication and characterization of single iridium-based mercury UMEs.^{28,29}

We describe here the microlithographic fabrication and analytical demonstration of an UME array which combines the advantages of the mercury electrode, iridium-based

mercury electrode, ultramicroelectrodes, and multielement array electrodes. The Ir-based Hg UME array displays the same unique and stable properties as the single Ir-based Hg UME previously described⁸ but with the added advantages of an increased signal, a well-defined geometry, the high reproducibility of array geometry from IC to IC, the possibility for incorporation of on-board microelectronics with increased bandwidth and high stability, and the eventual availability as a low-cost device for both basic studies and application to environmental or process monitoring.

EXPERIMENTAL SECTION

Electrochemical Apparatus. Chronoamperometric and square wave anodic stripping voltammetry (SWASV) experiments were carried out with an EG&G PAR Model 273 potentiostat/galvanostat (EG&G PAR, Princeton, NJ) interfaced to a DEC p420-SX microcomputer and using the Model 270 software (EG&G PAR, Princeton, NJ). All voltammetric experiments were performed using a two-electrode system consisting of a working UME array (UMEA) and the custom-fabricated reference electrode described below. Optical *in situ* microscopic observations of the electrodes were made with a Metaval-H (Leco/Jena) inverted polarizing microscope equipped with a video imaging and processing system and a 35-mm Pentax camera for microphotography.

Reference Electrodes. The use of UMEs allows SWASV measurement to be conducted with very little or no added supporting electrolyte. Under these conditions, it is very important for the reference electrode itself not to introduce any electrolyte into the sample. The commonly used saturated calomel reference electrodes contain a liquid internal electrolyte and a fiber or Vycor junction which can leak significant amounts of Cl⁻, even when a sample-filled bridge is used. To overcome this leakage problem, we fabricated and used a *solid-state Nafion-coated Ag/AgCl pseudoreference electrode* (SSNE) containing no internal liquid electrolyte or flow junctions.³⁰ Unless otherwise indicated, all potentials are the SSNE (~+220 mV vs SCE). The exception to this was the use of a sodium-saturated calomel reference electrode (SSCE) for deposition of the mercury hemispheres on the iridium disks.

Microlithographic Fabrication of the Iridium Array. The UME array was fabricated on a standard 4-in. silicon wafer substrate. The individual fabrication steps are fully described elsewhere³¹ and only the major steps briefly summarized below. The wafers were cleaned, and a thin layer of silicon dioxide was thermally grown on the surface. After being coated with photoresist and patterning, iridium was dc magnetron sputtered onto the surface to define the UME array elements. An interconnect layer of gold was then deposited to form the conductive traces between the UME locations and the bond pads. Due to its chemical inertness, iridium cannot be chemically or plasma etched and thus a liftoff process must be used to leave the desired iridium pattern on the substrate. In order to protect and insulate the conductors from the aqueous analyte solutions, a low-temperature plasma enhanced chemical vapor deposition (PECVD) process was used to apply a coating of silicon nitride (Si_xN_yH_z). Previous studies have

(25) Aoki, K.; Takuda, K.; Matsuda, H. *J. Electroanal. Chem.* 1987, 225, 19-26.

(26) Kounaves, S. P.; Buffle, J. *J. Electrochem. Soc.* 1986, 133, 2495-2498.

(27) Guminski, C.; Galus, Z. In *Solubility Data Series—Metals in Mercury*; Hirayama, C., Guminski, C., Galus, Z., Eds.; Pergamon Press: Oxford, UK, 1986; Vol. 25.

(28) Kounaves, S. P.; Deng, W. *J. Electroanal. Chem.* 1991, 301, 77-85.

(29) De Vitre, R. R.; Tercier, M.-L.; Tsacopoulos, M.; Buffle, J. *J. Anal. Chem. Acta* 1991, 249, 419-425.

(30) Deng, W.; Kounaves, S. P. To be submitted for publication in *Anal. Chem.*

(31) Kovacs, G. T. A.; Storment, C. W.; Kounaves, S. P. Submitted for publication in *Sens. Actuators B*.

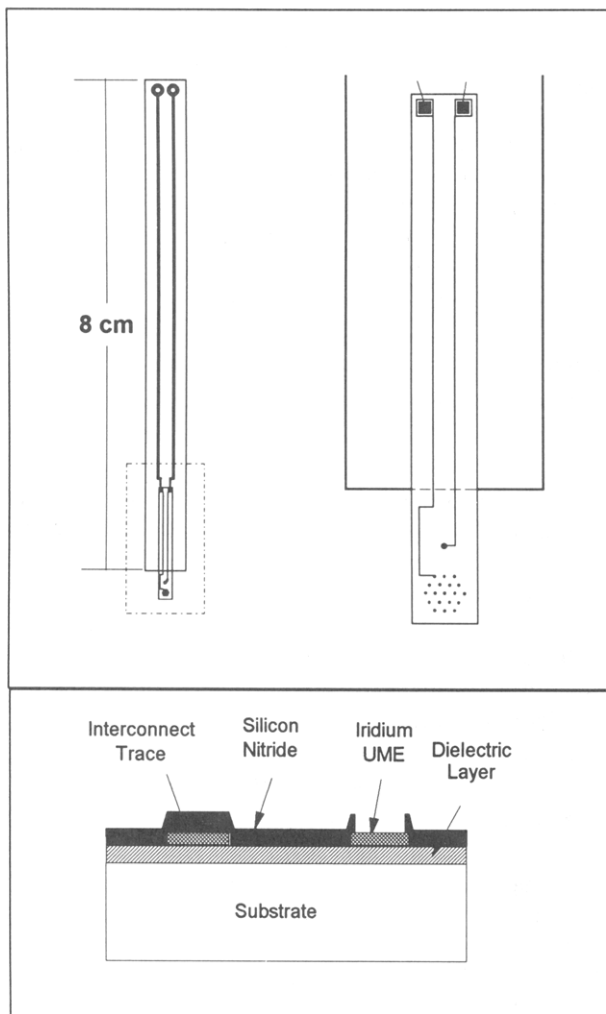


Figure 1. Diagrammatic view of (a, top) the 19-element array mounted on the PC board and (b, bottom) the structure of the Ir UME and traces on the silicon wafer.

shown that silicon nitride is an excellent passivation layer for this purpose.³² The silicon nitride was then selectively plasma etched from the iridium UME locations to give the desired UME sizes and patterns. The individual demarcated UME arrays and bond pad assemblies were cut into 2 mm × 16 mm chips, attached, and connected to a 80 mm × 6 mm custom-designed printed circuit (PC) board. A diagrammatic view of the 19-element IC array mounted on the PC board is shown in Figure 1a, with Figure 1b showing the structure of a single UME on the silicon wafer. Two UME array designs were utilized in this work: a prototype array consisting of 16 array elements in two lines spaced 45 μm from each other, each of which could be either individually controlled or connected together to act as a single array. This UME array was used only for a few initial experiments. The other UME array design consisted of 19 disk UMEs each measuring 10 μm in diameter and spaced 300 μm center to center from its nearest neighbor. This spacing was used to ensure that there would be no overlap of the individual diffusion layers during the time scale of any of the electroanalytical technique to be used. Unless otherwise indicated, this array design was used for all experiments and analyses.

(32) Kwon, O. H. A Microelectrode with CMOS Multiplexer for an Artificial Ear. Doctoral Dissertation, Technical Report No. G909-3, Stanford University, October 1986.

Deposition of the Mercury. Prior to analytical use, the tip of the IC containing the iridium UME array was placed in a solution containing 8×10^{-3} M Hg(II) in 0.1 M HClO₄ and a potential of 0.2 V vs SSCE was applied for a specified time. The geometry of the deposited mercury can be controlled from a thin film to almost a sphere, depending on the deposition parameters; however, because of ruggedness and stability a hemispherical or spherical segment geometry is preferred. The amount of mercury deposited was determined from the deposition charge. For the 19-element UME array, a deposition charge of 260 μC resulted in a hemispherical mercury coverage. After deposition of mercury, the electrode was removed from the Hg(II) solution, rinsed carefully with deionized water, and then transferred to the sample cell. For optimum performance, the mercury was replated at the beginning of each day. When stored in deionized water, the mercury could be maintained in satisfactory working condition for several days, and with the application of a slightly negative potential, it could be maintained for at least 7 days. The mercury was removed by dipping the tip of the IC into concentrated nitric acid for 3–5 s and then rinsing with deionized water.

Reagents. All solutions were prepared with 18.2 MΩ·cm deionized water from a Barnstead Nanopure system (Barnstead Co., Newton, MA). The acetate buffer solutions were prepared with 99.99+% ammonium acetate and acetic acid and the pH adjusted to 4.5 with addition of HClO₄ (Aldrich). Metal solutions were prepared from 99.9995% Cu(NO₃)₂, Cd(NO₃)₂, Hg₂(NO₃)₂ (ALFA-Johnson Matthey, Ward Hill, MA), and Pb(NO₃)₂ (Aldrich). All other solutions were prepared from ACS reagent grade chemicals. The spring water sample was obtained from a previously unopened 1 gal bottle of Poland Spring Water (Poland Spring, ME).

RESULTS AND DISCUSSION

A thorough characterization was undertaken to ensure that the iridium UME array performed as a single UME and that the microlithographic configuration did not introduce artifacts into the electroanalytical techniques to be used.

Individual vs Array UME Behavior. To maintain all of the desirable properties of UME behavior, the array of UMEs must behave as a single UME. Thus, the diffusion field of each UME must be isolated from all neighboring UMEs during the time frame of the experiment, otherwise the overlap of individual spherical diffusion layers will result in the appearance of a larger linear diffusion layer covering the entire area of the array and a response characteristic of such diffusion. The absence of this behavior for both of the arrays was demonstrated by several techniques. Since the data led to the same conclusions for both arrays, only the results of the chronoamperometry and chronocoulometry are presented for the 19-element iridium disk UME array and only those for SWASV are presented for the 16-element mercury hemisphere UME array.

For the 19-element Ir UMEA, the chronoamperometric curves were obtained in a solution containing 0.1 M K₃Fe(CN)₆ and 0.2 M KNO₃. The potential was stepped from 500 to –600 mV to ensure total diffusion control. The curves were taken for total time periods varying from 16 ms to 1000 s. Figure 2 shows the current plotted against time for the

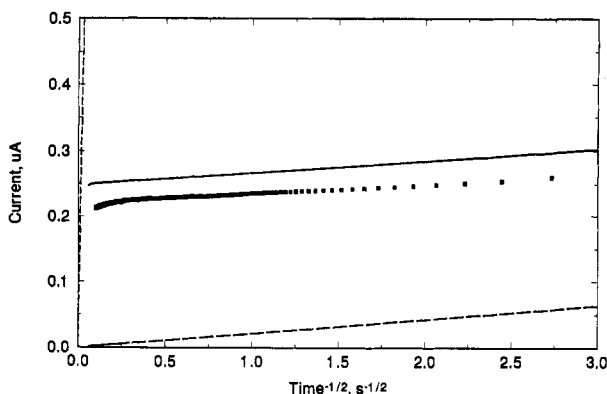


Figure 2. Chronoamperometric current plotted against time for the experimental (■) and the theoretical currents (—). Also shown is the calculated response for linear diffusion to a single electrode of the same total geometric area as the entire UME array (---) and for spherical diffusion to a single UME of the same active area (—). Conditions: 0.1 M $\text{K}_3\text{Fe}(\text{CN})_6$ in 0.2 M KNO_3 . Potential stepped from 500 to -600 mV for $t = 1000$ s.

experimental (■) and the theoretical currents (—) calculated using the equations of Shoup and Szabo³³ for an UME disk array with the same geometric configuration and with a diffusion coefficient of 6.8×10^{-6} cm²/s. Other than a slight difference of the ~30 nA (which will be accounted for below), the two curves are the same. For comparison, Figure 2 also shows the calculated response for linear diffusion to a single electrode of the same total geometric area as the entire UME array (---) and for spherical diffusion to a single UME of the same active area (—).

Chronocoulometric plots of the same data, but as charge (q) vs the square root of time ($t^{1/2}$), for the shortest and longest time periods are shown in Figure 3. For linear diffusion, a plot of q vs $t^{1/2}$ should give a linear relationship. As can be seen, the UME displays spherical steady-state diffusion from $t^{1/2} \approx 1.2$ ms^{1/2} to at least $t^{1/2} = 32$ s^{1/2} but exhibits linear diffusion for $t^{1/2} \lesssim 1.2$ ms^{1/2}. Even though we would expect that at short enough times the diffusion layer would indeed be planar, calculations show that for an inlaid disk UME, with the radius used here, planar diffusion should not be significant for $t^{1/2} > 0.5$ ms. As will be shown later, the above result is most likely due to the fact that the UMEs comprising the array are effectively recessed and not truly inlaid.

The 16-element iridium disk UME array was prepared as described above to provide a 16-element mercury hemisphere UME array for use with the SWASV experiments. The array was tested using a solution of 1×10^{-6} M Pb^{2+} in 0.1 M acetate buffer, a deposition time of 60 s, a square wave amplitude (half peak to peak) $E_{sw} = 25$ mV, a step height $\Delta E_s = 5$ mV, and a square wave frequency of $f = 120$ Hz. Figure 4a shows the forward (○), reverse (□), and net (■) current response using only one of the Hg UME array elements while Figure 4b shows the response using all 16 Hz UMEs of the array with the same exact conditions and solution. The peak current for a single UME is ~35 nA while for the 16 UME array it is ~530 nA (~15 times as great). Even though the array peak current signal shows a ~5% loss, the overall peak shape and characteristics (peak potential, E_p and peak width, $W_{1/2}$) remain basically the same as those observed for a single

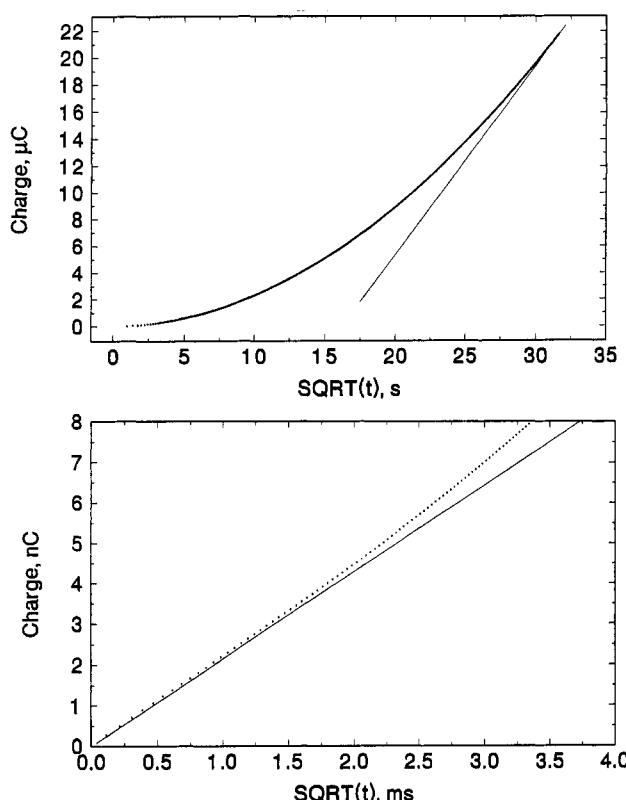


Figure 3. Chronocoulometric plots of data in Figure 2, but as charge (q) vs the square root of time ($t^{1/2}$), for the (a, top) longest and (b, bottom) shortest experimental time periods. For linear diffusion, a plot of q vs $t^{1/2}$ should give a linear relationship. The UME array displays spherical steady-state diffusion from $t^{1/2} \approx 1.2$ ms^{1/2} to at least $t^{1/2} = 32$ s^{1/2} but exhibits linear diffusion for $t^{1/2} \lesssim 1.2$ ms^{1/2}.

electrode and conform to SWASV theory. This is very important since it indicates that there is no interference or overlap between the individual Hg UMEs and that the array as a whole responds as a single Hg UME.

Effect of Recessed UME Array Disks. Because of the microlithographic technique used to fabricate the iridium UME array, the UME disks are not plane (inlaid) in relation to the surrounding insulating surface but are effectively recessed as shown in Figure 1b. Such geometry means that the diffusion layer must "climb" out of a "well" before it can begin to assume a spherical configuration. The effects of this geometry on the electroanalytical response can be seen in two situations. First, Bond et al.³⁴ have shown that the steady-state current at a recessed disk UME (i_r) will be less than that at an equivalent inlaid disk UME (i_i). For an UME with a radius of 5 μm , the silicon nitride layer of 0.8- μm thickness provides enough of a recessed depth to reduce the steady-state current by ~10% compared to an inlaid UME. This may explain the slightly lower measured current as compared to theory that was seen in Figure 2. Second, since the thickness of the linear diffusion layer δ_L as a function of time is given by $\delta_L = (\pi D t)^{1/2}$, the diffusion layer will begin to emerge from a recessed channel of 0.8- μm depth ~0.5 ms after application of the reduction potential. These data correlate well with the experimental chronocoulometric results shown in Figure 3b, where the curve remains linear up to at least 0.6 ms. Thus,

(33) Shoup, S.; Szabo, A. J. *Electroanal. Chem.* 1984, 160, 19–26.

(34) Bond, A. M.; Luscombe, D.; Oldham, K.; Zoski, C. J. *J. Electroanal. Chem.* 1988, 249, 1–14.

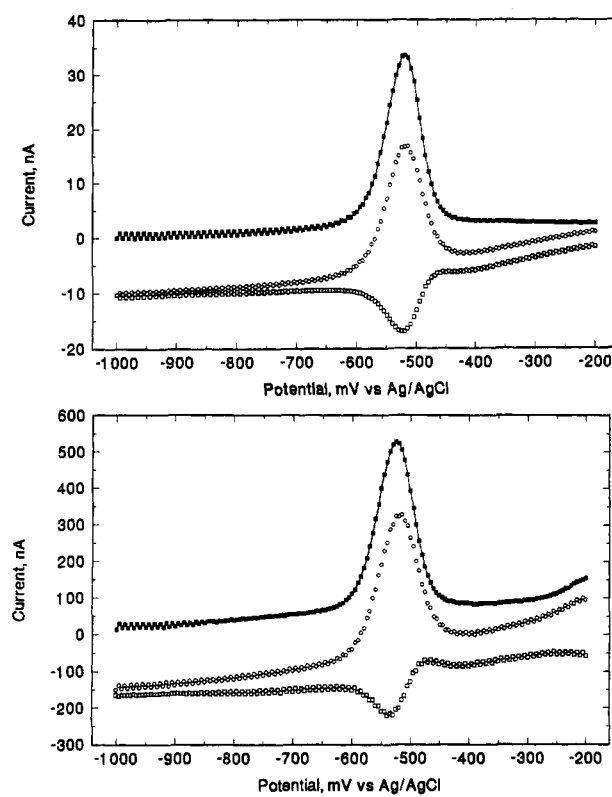


Figure 4. Square wave ASV curves showing the forward (O), reverse (□), and net (■) current response using (a, top) only one of the Hg UME array elements and (b, bottom) all 16 Hg UMEs of the array, under the same conditions and solution. Conditions: 1×10^{-6} M Pb²⁺ in 0.1 M acetate buffer, $t_d = 60$ s, $E_{sw} = 25$ mV, $\Delta E_s = 5$ mV, and $f = 120$ Hz.

for experiments which take place at time frames well beyond 1 ms (and assume that spherical diffusion is in effect), the recessed UMEs will not introduce any significant deviation from the steady-state response expected from an equivalent inlaid UME. It is interesting to note that, for an inlaid UME, spherical diffusion will already account for more than 10% of the total current after a time of only ~ 100 μ s.³⁴

Comparison of SWASV at the UMEA to Theory. Since no previous studies appear in the literature for SWASV at an array of hemispherical mercury UMEs formed on an array of microlithographed iridium disks, the experimental results were compared with the theoretical response. The experimental data (O) were obtained using a solution of 8×10^{-8} M Cd²⁺ in 0.2 M KNO₃ and 0.002 M acetate buffer, with a deposition time of 30 s, $E_{sw} = 25$ mV, $\Delta E_s = 5$ mV, and $1 \text{ Hz} < f < 5000$ Hz. The net peak current (i_p), peak potential (E_p), and peak half-width ($W_{1/2}$) are shown plotted in Figure 5A–C, respectively, as a function of the dimensionless parameter ρ , with $\rho = r f^{1/2} / D_R^{1/2}$ where r is the radius of the mercury hemisphere (5×10^{-4} cm), f is the square wave frequency, and D_R is the diffusion coefficient of Cd⁰ in mercury (1.5×10^{-5} cm²/s). The theoretical curves (—) were calculated using the theory for SWASV at a hemispherical mercury UME.³⁵ Even though the theory is for a single UME, the observed behavior that the array does act as a single UME allows the application of this theory with relative confidence. For i_p and E_p , the experimental values were normalized to the

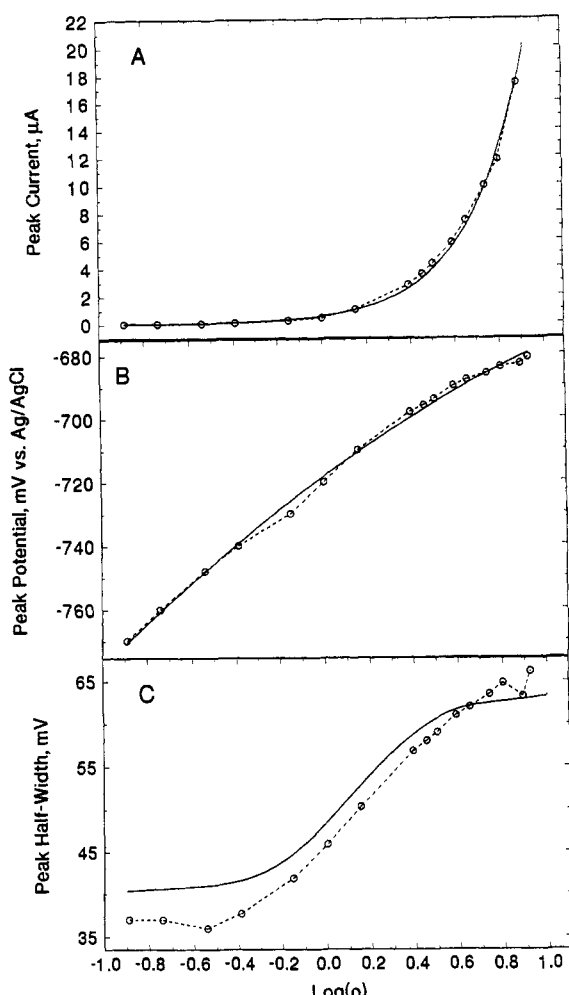


Figure 5. (A) Net peak current (i_p), (B) peak potential (E_p), and (C) peak half-width ($W_{1/2}$) of the experimental data (O) and theoretical curves (—) plotted as a function of the dimensionless parameter $\rho = r f^{1/2} / D_R^{1/2}$ with $r = 5 \times 10^{-4}$ cm and D_R (Cd⁰/Hg) = 1.5×10^{-5} cm²/s. Conditions: 8×10^{-8} M Cd²⁺ in 0.2 M KNO₃ and 0.002 M acetate buffer, $t_d = 30$ s, $E_{sw} = 25$ mV, $\Delta E_s = 5$ mV, and $1 \text{ Hz} < f < 5000$ Hz.

theoretical values before the fit was made. This is necessitated since i_p requires the exact concentration of the reduced metal in the mercury and E_p is in relation to a relative reference potential. In all cases, the fit of the experimental data to theory was rather good, indicating that the behavior of the hemispherical mercury UME array is as predicted by theory and also, more importantly, conforms to that of a single hemispherical mercury UME.

SWASV Analysis of Metal Ions in Water. The analytical utility of the UMEA was demonstrated by analysis for added Cd²⁺, Pb²⁺, and Cu²⁺ in neat spring water. Without any electrolyte or buffer added, successive additions of Cd²⁺, Pb²⁺, and Cu²⁺ were made to give concentrations of 5, 10, 15, 20, and 25 ppb of each metal. The solution was neither deoxygenated nor stirred during the analysis, and no equilibrium period was allowed between the deposition and stripping step. The SWAVS parameters used were $E_{sw} = 25$ mV, $\Delta E_s = 5$ mV, and $f = 120$ Hz, a deposition potential of -1500 mV vs SSNE, and a deposition time of 260 s. As can be seen in Figure 6, the SWAVS peaks for Cd²⁺ and Pb²⁺ while not ideal in shape or separation are reasonably well defined for obtaining quantitative data. On the other hand,

(35) Liu, Z.; Deng, W.; Kounaves, S. P. Submitted for publication in *J. Electroanal. Chem.*

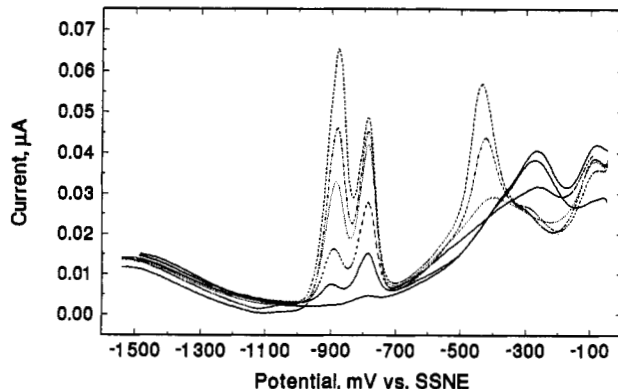


Figure 6. Square wave voltammograms for a test solution containing neat spring water with successive additions of Cd^{2+} , Pb^{2+} , and Cu^{2+} to give 5, 10, 15, 20, and 25 ppb concentrations of each metal. The solution was neither deoxygenated nor stirred during the analysis, and no equilibration period was allowed between the deposition and stripping step. Conditions: $E_{\text{sw}} = 25 \text{ mV}$, $\Delta E_s = 5 \text{ mV}$, $f = 120 \text{ Hz}$, $E_{\text{dep}} = -1500 \text{ mV}$ vs SSNE, and $t_d = 260 \text{ s}$.

the peak for Cu^{2+} presents a somewhat more complicated picture. For the blank and the 5 ppb addition, no oxidation peak for Cu^{2+} can be seen. The peak at $\sim -300 \text{ mV}$ appears to be similar to that previously identified as being most likely due to some form of natural organic matter in the spring water sample.⁷ As the concentration of Cu^{2+} is increased to 15 ppb the "organic" peak begins to decrease. With the subsequent standard additions of Cu^{2+} giving 20 and 25 ppb, the "organic" peak decreases and is overwhelmed by that for Cu^{2+} at -400 mV . A comparison of the voltammograms for the spring water sample with those obtained from a buffered solution showed that the Cu^{2+} and Pb^{2+} oxidation peaks of the former were shifted about 100–150 mV cathodic. The peak for Cd^{2+} however, remained at -900 mV in both cases. Since no electrolyte or buffer was added to the spring water sample, this shift is probably due to either the formation of hydroxide or carbonate species at the surface of the electrodes during the stripping step or the complexation of the Pb^{2+} and Cu^{2+} by the naturally occurring ligands. Plots of peak current vs concentration yielded straight lines with intercepts at zero for all three metals.

CONCLUSIONS

The microlithographically fabricated iridium-based mercury UME array shows a response with chronoamperometry and square wave ASV, equivalent to that expected for a single UME, with multiplication of the faradaic current proportional to the number of UMEs in the array and with no overlap of the diffusion fields. The deposition of mercury on the iridium disks appears stable, with no resulting degradation or dissolution of the iridium pads even after several days of use. No stray capacitance effects were observed and only minor effects due to the recessed position of the UME disk. Overall, the microcircuit-based mercury UME array performed excellently and gave analytical results with square wave peak widths and peak potentials as predicted by theory. The Hg UME array can be used for routine determinations as any mercury film electrode can but with the added advantages conferred by the UME configuration. It can also be used in natural water samples without any added electrolytes for determination of Cd^{2+} , Pb^{2+} , and Cu^{2+} .

We are currently fabricating a version of this sensor with an integrated on-board digital potentiostat and reference electrode. Such a sensor could be made part of a hand-held device for on-site and/or in situ analytical measurements of environmentally important metals amenable to ASV analysis.

ACKNOWLEDGMENT

Initial development of the microlithographic fabrication technology for the iridium array was supported in part by the Stanford Center for Integrated Systems Seed and Research Thrust Grants, the U.S. Department of Veterans Affairs, and funds from the Robert N. Noyce Family Faculty Scholar Chair (G.T.A.K.). The research described here was supported in part by grants from the U.S. Environmental Protection Agency, the Northeast Hazardous Substance Research Center, the EG&G Princeton Applied Research Corp., and the National Science Foundation (CHE-925871).

Received for review May 24, 1993. Accepted November 4, 1993.®

• Abstract published in *Advance ACS Abstracts*, December 1, 1993.